IIETA International Information and Engineering Technology Association
Advancing the World of Information and Engineering

Mathematical Modelling of Engineering Problems
Vol. 13, No. 6, June, 2026, pp. 905-913
Journal homepage: http://iieta.org/journals/mmep

Finite Element Modeling of Pulsatile Hemodynamics in an Idealized 2D Rigid Stenosed Bifurcated Coronary Artery

Howlader Jannatul Nieem, Chinmayee Podder*, Sidratul Muntaha

Department of Mathematics, University of Barishal, Kornokathi, Barishal 8254, Bangladesh

Corresponding Author Email: cpodder@bu.ac.bd

https://doi.org/10.18280/mmep.130601

Received: 12 April 2026
Revised: 5 June 2026
Accepted: 16 June 2026
Available online: 15 July 2026

Keywords:
bifurcated artery, finite element method, hemodynamic behavior, Oscillatory Shear Index, pulsatile blood flow, stenosis, wall shear stress

ABSTRACT

This study investigates the hemodynamic characteristics of pulsatile blood flow in an idealized 2D rigid bifurcated coronary artery with 50% stenosis in the parent artery and both daughter arteries under laminar flow conditions using the finite element method (FEM). The finite element approach in COMSOL Multiphysics 6.2 software is used to simulate the unsteady Navier-Stokes equations for physiological blood flow using both Newtonian and non-Newtonian (Carreau) fluids. The results demonstrate pronounced temporal variations in hemodynamic parameters. Peak velocity decreases by approximately 96–97% from systole to diastole. The findings indicate that there are notable temporal differences in the hemodynamics of the parameters under study during the cardiac cycle. There is a 96.4% and 97.0% drop in peak velocity between systole and diastole in the Newtonian and non-Newtonian models, respectively. In terms of peak pressure, there is a dramatic drop from approximately 9.2–9.3 kPa during systole to 0.355–2.26 Pa during diastole, whereas wall shear stress (WSS) falls from 651 Pa to 3.06 Pa. This shows that the development of multi-site severe stenosis changes the local fluid dynamics significantly, whereas the non-Newtonian property of the blood impacts the flow. This will assist in gaining deeper insights into disease progression in stenosed bifurcated arteries.

1. INTRODUCTION

Cardiovascular diseases are a common cause of illness and death around the world. In particular, atherosclerosis can be considered one of the key pathologies, which is associated with the formation of lipid-laden fibrotic plaques in the wall of arteries. The expansion of these plaques results in narrowing of the artery lumen, affecting hemodynamic functions. Shear thinning fluid model predicts better results of velocity and flow rate compared to Newtonian model while giving the same wall shear stress (WSS) in stenotic arteries. The geometry of stenosis and flow conditions have an impact on the hemodynamics of arteries and this makes computational models an effective tool for the study of stenotic flow. In case of pulsatile flow, multi-stenotic conduits show local acceleration, then deceleration after stenosis and large pressure gradients [1-3]. The geometry and stenosis severity can have an effect on the blood hemodynamic inside the artery. The asymmetry in the stenosis leads to changes in the flow pattern, pressure recovery, and the resistance of the flow, which makes the geometrical information very important in diagnosis. More stenosis severity leads to a higher velocity of flow, pressure drop, and WSS [4, 5]. Comparison of Newtonian, power-law, and Carreau models for flow in the Left Coronary Artery (LCA) reveals that the non-Newtonian characteristics have a major impact on velocity, pressure gradient, and WSS. They also cause less turbulence and vortices, making a more accurate hemodynamic analysis possible in the stenosed artery [6, 7]. Pulsatile flow through stenotic arteries can produce an abrupt pressure decrease at the stenosis and oscillatory WSS, while Carreau-Yasuda modeling helps describe the shear-thinning behavior of blood. In coronary artery bifurcations, low and oscillatory WSS is another important factor in the formation of atherosclerotic plaques [8, 9]. The coronary hemodynamics are affected to a great extent by the geometry of the bifurcation as well as individual anatomical features. Other factors like vessel geometry, cardiac cycle mechanics, and blood rheology affect coronary blood flow as well. These results demonstrate that computational analysis can be very useful in studying disturbed flow and stent design [10, 11]. Recent reviews have emphasized the importance of blood rheology, boundary conditions, fluid-structure interaction, and accurate stenosis modeling in Computational Fluid Dynamics (CFD)-based assessments of coronary hemodynamics [12].

While previous studies have investigated the effects of stenosis in bifurcated arteries, the interaction between stenosis of the parent artery and the two daughter arteries under pulsatile flow has not yet been fully addressed. In order to fill this knowledge gap, this paper presents a finite element analysis of a bifurcated LCA with 50% stenosis of the parent artery and both daughters under systolic and diastolic conditions using both the Newtonian and non-Newtonian (Carreau) models of blood.

2. GEOMETRIC MODELING

2.1 Model construction

Figure 1 shows the geometry of the bifurcated artery modeled using SolidWorks. The parent artery has a 4 mm inlet, while the two daughter branches have 2 mm outlets. Fillets were added to the area of stenosis to eliminate sharp corners and to enable a smooth flow transition in the vessel wall. The dimension of the parent artery was taken to be 28 mm, while that of the daughter arteries was taken to be 22 mm [13]. The whole design of the model was meant to mimic the anatomical structure of the LCA.

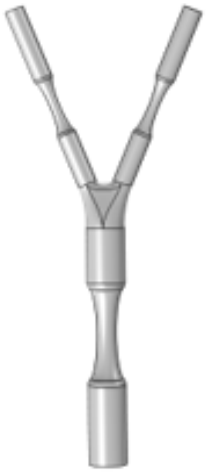

Figure 1. Bifurcated artery with 50% stenosis in the parent and daughter arteries

2.2 Governing equation and boundary conditions

The unsteady form of the governing equation for an incompressible fluid is given as follows [7]:

$$\rho\left(\frac{\partial \boldsymbol{u}}{\partial t} + \boldsymbol{u}.\nabla\boldsymbol{u}\right) = -\nabla p + \nabla.\boldsymbol{\tau}(\boldsymbol{u}) + \mathbf{f} \tag{1}$$

$$\nabla.u = 0 \tag{2}$$

where, ρ is the fluid density, t is time, p is pressure, $\mathbf{f}$ is the external body force per unit volume (set to zero), $\boldsymbol{\tau}$ is the viscous stress tensor. For a Newtonian, incompressible fluid, $\boldsymbol{\tau}$ is defined as:

$$\boldsymbol{\tau} = 2\mu\boldsymbol{D} \tag{3}$$

where, μ is the Newtonian viscosity, and $\boldsymbol{D}$ is the rate of deformation tensor defined as:

$$\boldsymbol{D} = \frac{(\Delta\boldsymbol{u} + \Delta\boldsymbol{u}^T)}{2} \tag{4}$$

For non-Newtonian fluid $\boldsymbol{\tau}$ can be written as:

$$\boldsymbol{\tau} = 2\mu_{\text{eff}}(\dot{\gamma})\mathbf{D} \tag{5}$$

where, $\dot{\gamma}$ refers to the shear rate defined as

$$\dot{\gamma} = \sqrt{2\mathbf{D}:\mathbf{D}} \tag{6}$$

And $\mu_{\text{eff}}(\dot{\gamma})$ is the constitutive shear rate function which describes the effective viscosity in terms of $\dot{\gamma}$.

2.3 Blood properties

In this study, unsteady-state blood flow was examined using both Newtonian and non-Newtonian models. Initially, blood was considered a Newtonian fluid with a density of 1060 kg/m^3 and a dynamic viscosity of 0.00345 Pa s [14, 15]. Furthermore, blood was modeled as a non-Newtonian fluid, and its viscosity was computed using the Carreau model. The constants were determined with reference to the study by Konstantinos Tzirakis et al. [14]. The Carreau model is defined by Eq. (7), $\mu_\infty = 0.00345, \mu_0 = 0.056, \lambda = 3.313, n = 0.3568$ [14]. Density, $\rho = 1060\ \text{kg/m}^3$ [15].

$$\mu(\dot{\gamma}) = \mu_\infty + \frac{(\mu_0 - \mu_\infty)}{[1 + (\lambda\dot{\gamma})^2]^{(1-n)/2}} \tag{7}$$

The Carreau model was selected because it accurately represents the shear-thinning behavior of blood over a wide range of shear rates and has been widely adopted in computational hemodynamic studies.

2.4 Boundary condition

In the present study, considering simple pulsatile flow, we have taken inlet velocity, $u(t) = 1 + \sin\left(2\pi\frac{t}{T}\right)$ [16], and outlet pressure, p = 0 Pa.

In this study, the Oscillatory Shear Index (OSI) was calculated over one complete cardiac cycle (0–1 s) using the transient WSS obtained from the time-dependent simulations. The OSI is defined as:

$$OSI = \frac{1}{2}\left(1 - \frac{|\int_0^T \tau_w(t)\,dt|}{\int_0^T |\,\tau_w(t)|dt}\right)$$

where, T is the cardiac cycle period and τ_w is the instantaneous WSS.

A time-dependent fully coupled solver was employed with a fixed time-step size of 0.01s and a relative convergence tolerance of 0.005. Based on the mean inlet velocity, the Reynolds number was approximately 1229, indicating laminar flow conditions.

2.5 Grid independence test

Since the present study deals with unsteady pulsatile flow, a grid independence test was performed using COMSOL 6.2 at t = 0.25 s, corresponding to a peak systolic phase where flow dynamics are most active. Maximum velocity was chosen as the reference quantity to assess the sensitivity of the solution to mesh refinement. As presented in Table 1, for the Newtonian model, the maximum velocity difference between Mesh 4 (9693 elements) and Mesh 5 (22047 elements) is minimal. These results collectively indicate that grid independence has been achieved. In contrast, for the non-Newtonian model, the maximum velocity difference between Mesh 4 (9693 elements) and Mesh 5 (22047 elements) is minimal. These results also collectively indicate that grid independence has been achieved.

Table 1. Mesh convergence analysis of maximum velocity in Newtonian and non-Newtonian flow at t = 0.25 s

Newtonian			Non-Newtonian		
Mesh	Element	Max. velocity	Mesh	Element	Max. velocity
Mesh 1	3762	4.7059	Mesh 1	3762	4.7078
Mesh 2	4394	4.6712	Mesh 2	4394	4.6874
Mesh 3	6691	4.7023	Mesh 3	6691	4.7032
Mesh 4	9693	4.7897	Mesh 4	9693	4.7889
Mesh 5	22047	4.7955	Mesh 5	22047	4.7931

2.6 Model validation

The deviation observed could be due to variations in mesh resolution, solver setup, and boundary conditions. The numerical results presented in Table 2 show good agreement with the reference results. The similarities in flow pattern and velocity profile, particularly at areas of acceleration and recirculation, confirm the accuracy of the current model as illustrated in Figure 2.

Table 2. Quantitative comparison of velocity with reference data

Parameter	Reference Value (m/s)	Computed Value (m/s)	Relative Error (%)
Peak velocity	0.134216	0.13432	0.078

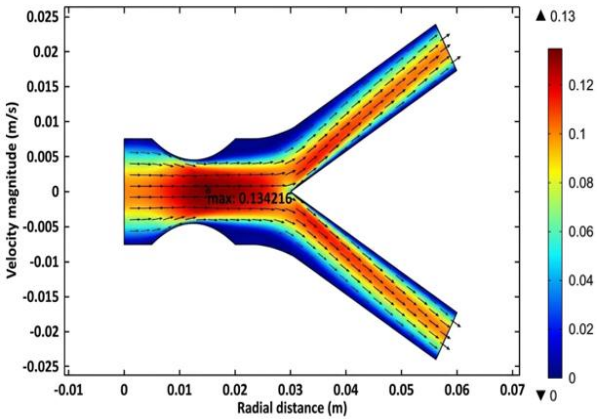

(a)

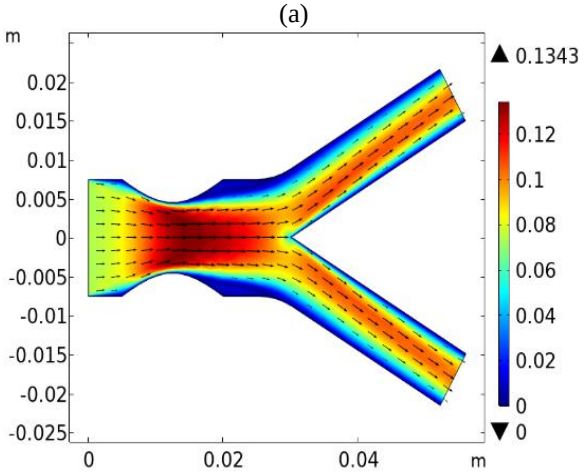

(b)

Figure 2. Velocity profile of (a) Zain and Ismail [17] and (b) present work (COMSOL 6.2)

3. RESULT AND DISCUSSION

3.1 Velocity and streamline profile analysis

Figure 3 shows the velocity distribution on the surface of the bifurcated artery model having 50% stenosis in the parent artery as well as both daughter branches at t = 0.25 s and t = 0.75 s under a Newtonian flow regime. In the case where t = 0.25 s, a highly prominent high velocity area forms in the stenotic parent artery, extending towards the bifurcation region. Since the stenosis is symmetrical for both daughter arteries, the symmetry of the flow pattern is maintained beyond the bifurcation.

A region of low velocity can be seen at t = 0.75 s upstream of the arterial stenosis in the parent artery. As the fluid flows through the channel further downstream, there is an increase in velocity to a higher level just before the onset of the bifurcation zone. After the division of the flow occurs downstream of the bifurcation zone, the velocity drops considerably in both branches, thus creating regions of low velocity downstream of the bifurcation. The velocity levels recorded are lower when compared to those recorded at t = 0.25 s. This is evident from the fact that stenosis at both the parent artery and the daughter arteries changes the velocity distribution at the bifurcation point. Velocity increases close to the bifurcation area but reduces in the daughter branches.

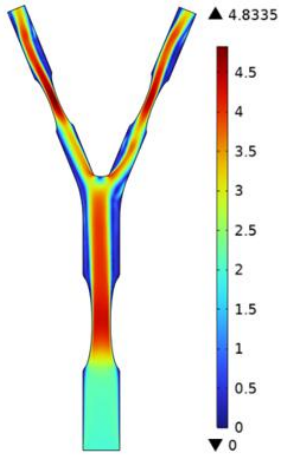

(a) t = 0.25 s

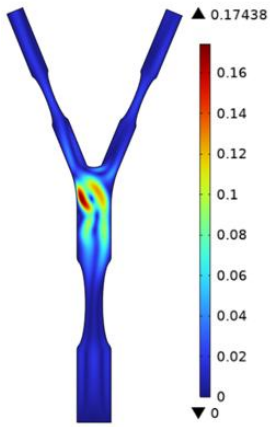

(b) t = 0.75 s

Figure 3. Velocity distributions at peak systole (t = 0.25 s) and end diastole (t = 0.75 s) (Newtonian)

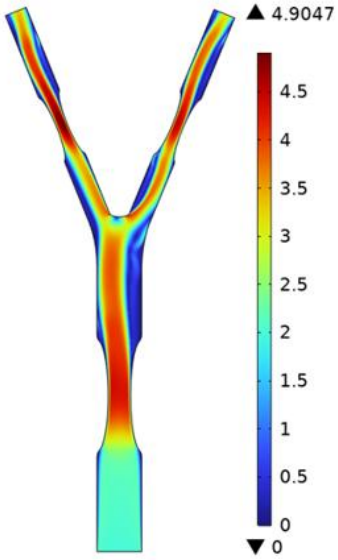

(a) t = 0.25 s

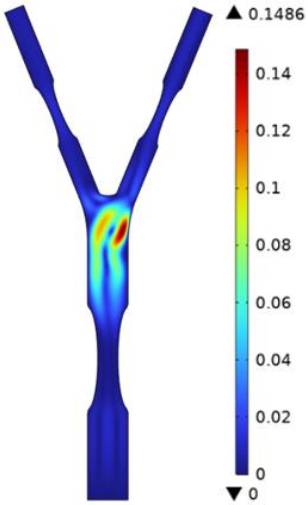

(b) t = 0.75 s

Figure 4. Velocity distributions at peak systole (t = 0.25 s) and end diastole (t = 0.75 s) (non-Newtonian)

Figure 4 shows the surface velocity magnitude variation of the bifurcated artery flow model, considering the 50% stenosis case in the parent artery and two daughter branches using the non-Newtonian fluid model at t = 0.25 s and t = 0.75 s. At t = 0.25 s, high-velocity regions are observed within the parent artery stenosis and its downstream section, extending toward the bifurcation. Due to the symmetric stenosis configuration, the velocity distribution remains nearly symmetric in both daughter branches. On the other hand, when t = 0.75 s, there are very small velocities registered within the pre-stenosis area as well as the stenosis area. The velocity becomes larger when the distance approaches the point of bifurcation, peaks close to the bifurcated area, then falls sharply into both daughter branches. The overall velocity at t = 0.75 s is smaller compared to the velocity at t = 0.25 s.

The low and high velocity flow zones in the stenosed bifurcated artery have been found to result in unique hemodynamic properties such as flow recirculation, stagnation, high WSS, and low pressure. In previous experimental and clinical studies, it has been suggested that the above flow properties are related to platelet activation, dysfunction of the endothelium, vascular remodeling, and atherosclerosis. Hence, the present results may give an insight into the flow environment linked to the progression of cardiovascular diseases.

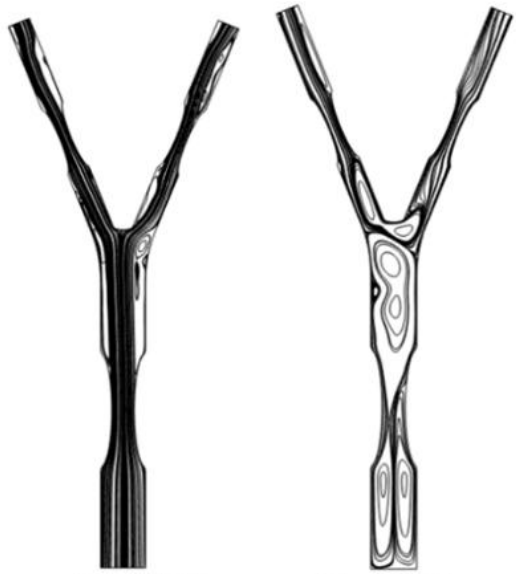

(a) t = 0.25 s (b) t = 0.75 s

Figure 5. Streamlines distributions at peak systole (t = 0.25 s) and end diastole (t = 0.75 s) (Newtonian)

Figure 5 illustrates the hemodynamic behavior of arterial stenosis under the Newtonian model at t = 0.25 s and t = 0.75 s. At t = 0.25 s, flow accelerates through the stenosis and experiences mild separation and a moderate downstream vortex, with recirculation at the entrance of the right daughter branch. The flow is highly complex, with multiple strong vortices dominating both daughter branches. Conversely, at t = 0.75 s, a nearly symmetric vortex forms in the upstream region and circular vortices appear in the downstream area. These findings suggest that both low and high velocity regions contribute to distinct but critical hemodynamic complications within diseased arterial geometries.

In Figure 6, at t = 0.25 s, from the stenosis throat to the bifurcation, a massive recirculation vortex is observed. Near the bifurcation apex, both branches exhibit moderate recirculation zones at their entrances. Smaller vortices are also observed further downstream, indicating that multiple stenoses contribute to vortex formation and flow disturbance. In contrast, at t = 0.75 s, the flow initiates with a recirculation zone just downstream of the inlet, spanning the entire pre-stenotic segment. A prominent vortex structure then forms from the stenosis throat to the bifurcation. Beyond the bifurcation moderate size recirculation zones emerge at the branch entries, followed by smaller disturbances along the downstream portions of each daughter artery. Large vortices present downstream of the stenosis lead to significant pressure and shear oscillations, indicative of a severely perturbed flow environment. Such hemodynamic features have been reported to be associated with adverse vascular environments in previous experimental and clinical studies [18].

Figure 7 illustrates the velocity profiles at the stenosis throat of the parent artery under Newtonian and non-Newtonian blood rheology models at t = 0.25 s and t = 0.75 s. At t = 0.25 s, both models produce nearly identical plug-like velocity

distributions with only minor differences in peak velocity, indicating a limited influence of blood rheology during this phase. In contrast, at t = 0.75 s, significant differences emerge between the two rheological models. The Newtonian model predicts considerably higher and more oscillatory velocity profiles, whereas the non-Newtonian model yields lower and smoother distributions due to the shear-dependent viscosity of blood. The effect of blood rheology is more pronounced than that of stenosis configuration, particularly during the later phase of the pulsatile cycle.

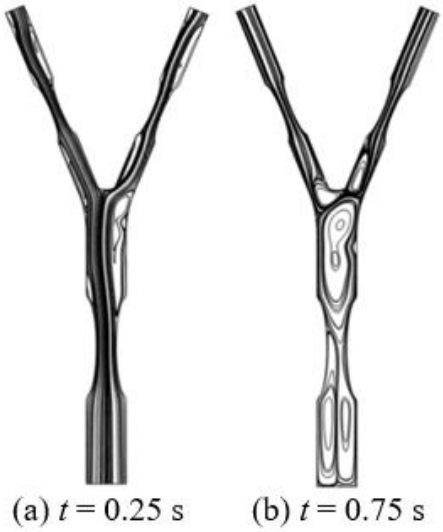

Figure 6. Streamlines distributions at peak systole (t = 0.25 s) and end diastole (t = 0.75 s) (non-Newtonian)

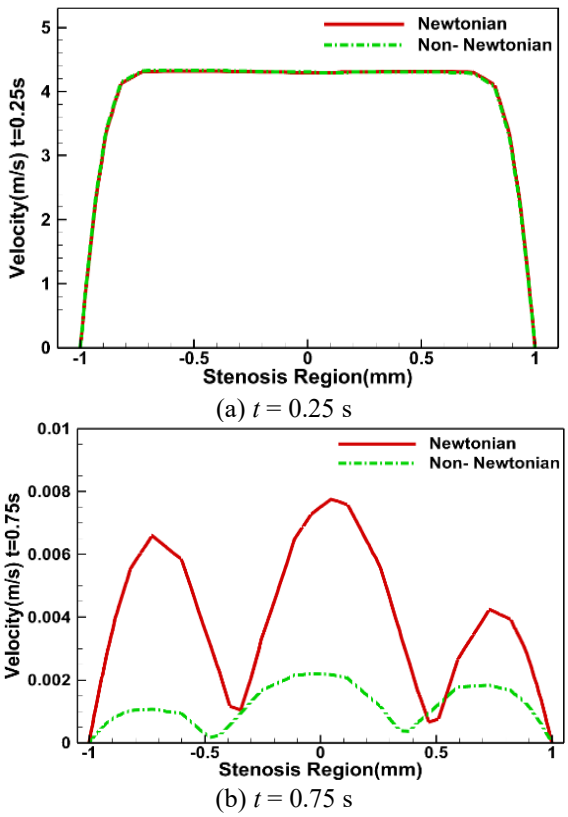

Figure 7. Velocity profiles at stenosis throat of parent artery for fluid rheology models at two pulsatile times

3.2 Pressure distribution analysis

In Figure 8, at t = 0.25 s, a pronounced pressure drop occurs at the stenosis throat that persists downstream, with only a moderate recovery near the bifurcation before decreasing again toward the outlets. Conversely, at t = 0.75 s, high inlet pressure with downstream drops and moderate pressure throughout, with the left daughter artery retaining the highest pressure. Excess pressure load on the arterial wall may cause localized dilation or structural weakening, especially where high pressure combines with high WSS. A substantial pressure drop may reduce downstream perfusion pressure, potentially affecting blood flow to distal vascular regions [19].

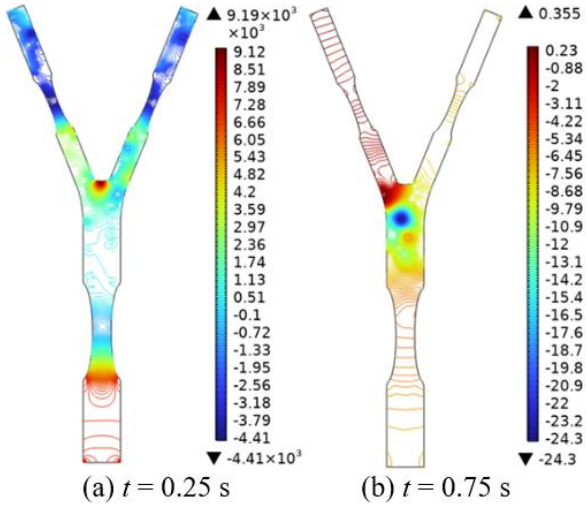

Figure 8. Pressure distributions at peak systole (t = 0.25 s) and end diastole (t = 0.75 s) (Newtonian)

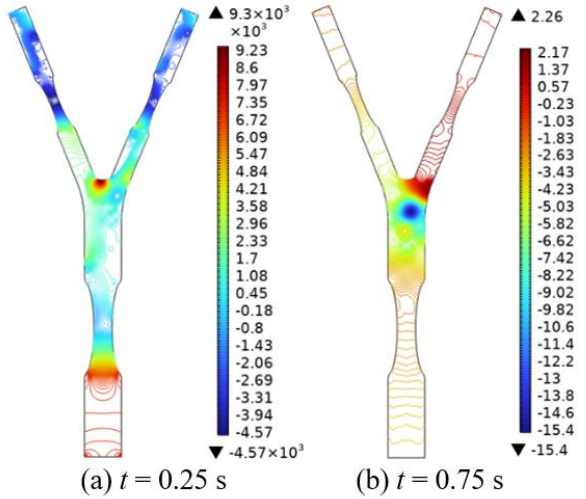

Figure 9. Pressure distributions at peak systole (t = 0.25 s) and end diastole (t = 0.75 s) (non-Newtonian)

In Figure 9, at t = 0.25 s under non-Newtonian flow, a very high upstream pressure is observed in the parent artery, followed by a pronounced pressure drop across the stenotic throat. A mild pressure recovery occurs near the bifurcation region, after which the pressure gradually decreases along both daughter arteries due to the presence of additional stenoses. The large pressure gradient generated by multiple stenotic segments indicates increased flow resistance and

hemodynamic burden on the arterial wall. Such sustained pressure gradients may contribute to vascular remodeling and further progression of arterial narrowing over time. In contrast, at t = 0.75 s, the pressure distribution becomes comparatively moderate. The pressure gradually decreases in the direction of the bifurcation. Yet, a relatively high-pressure area is evident in the right daughter artery just after the bifurcation. Pressure drops as the flow moves along the stenosed part. The left daughter artery maintains a more uniform moderate-pressure distribution. The downstream pressure reduction may facilitate flow separation and recirculation, creating disturbed flow conditions that can promote endothelial dysfunction and adverse vascular responses.

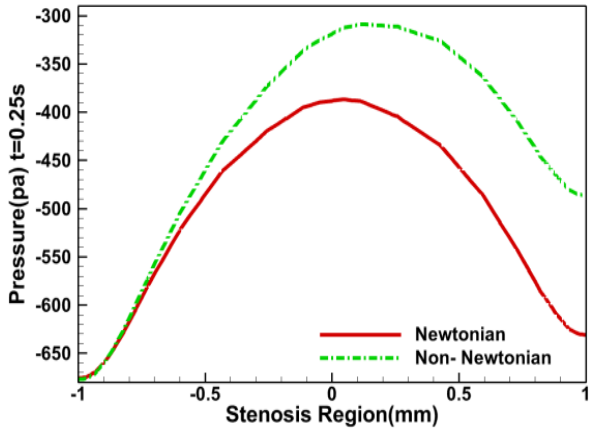

(a) t = 0.25 s

(b) t = 0.75 s

Figure 10. Pressure profiles at stenosis throat of parent artery for fluid rheology models at two pulsatile times

In Figure 10, at t = 0.25 s, during the peak systolic phase, the non-Newtonian model exhibits a sharp parabolic pressure profile, with the maximum at the center of the stenosis throat. The Newtonian model shows a similar trend, but with a smoother pressure profile and lower peak values at the stenosis throat. The non-Newtonian (Carreau) model predicts a slightly higher peak pressure compared to the Newtonian model. In contrast, at t = 0.75 s (end-diastolic phase), the pressure profiles flatten significantly for both Newtonian and non-Newtonian models, indicating a reduced pressure gradient due to lower flow rates. However, the Newtonian model consistently predicts a more negative pressure drop compared to the non-Newtonian model. This is because the Newtonian assumption ignores the shear-thinning nature of blood and maintains a constant viscosity. By accounting for viscosity variations with shear rate, the non-Newtonian model produces smoother pressure distributions and lower pressure extremes. As a result, adverse pressure gradients and associated hemodynamic stresses are reduced, yielding a more physiologically realistic prediction of blood flow in stenosed arteries.

3.3 Wall shear stress distribution analysis

Analyzing the WSS characteristics predicts stenosis diseases. Figure 11 shows that at t = 0.25 s (peak systole), moderate WSS is observed along the wall of the stenosis throat. Subsequently, minimum WSS is observed throughout the downstream and both branch arteries, except along the wall of the bifurcation. The highest WSS is found along the arterial wall in the bifurcation region. In contrast, at t = 0.75 s, moderate WSS is noticeable along the walls of the bifurcation region. High WSS is observed on the left arterial wall of the pre-bifurcation region, which may activate platelet-platelet attachment improves thrombosis in partially clogged blood arteries.

Figure 12 illustrates the WSS distribution for the bifurcated artery model with 50% stenosis in the parent artery and both daughter branches. At t = 0.25 s, moderate WSS is observed throughout the stenosed regions, while the highest WSS occurs near the bifurcation. In contrast, the central region of the parent artery exhibits relatively low WSS. At t = 0.75 s, low WSS is observed over most of the stenosed segments, whereas moderate WSS persists around the bifurcation. A localized high-WSS region appears along the right pre-bifurcation wall, indicating the presence of concentrated shear forces in this area. Compared with t = 0.25 s, the overall WSS magnitude decreases at t = 0.75 s due to the reduced flow rate during this phase of the pulsatile cycle. Previous research has revealed that low WSS is related to endothelial dysfunction and the development of atherosclerotic plaques. However, high WSS can lead to vulnerability and progression of the plaque, especially in areas experiencing high levels of shear stress on the walls.

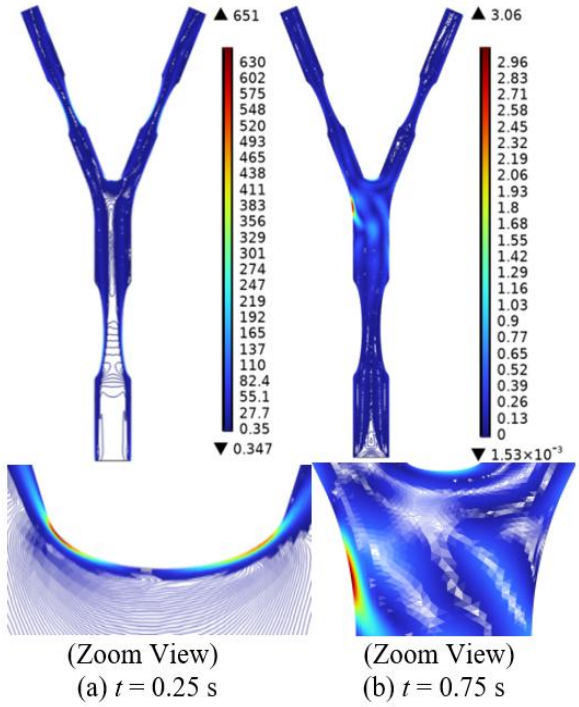

(Zoom View)
(a) t = 0.25 s

(Zoom View)
(b) t = 0.75 s

Figure 11. Wall shear stress (WSS) distributions at peak systole (t = 0.25 s) and end diastole (t = 0.75 s) (Newtonian)

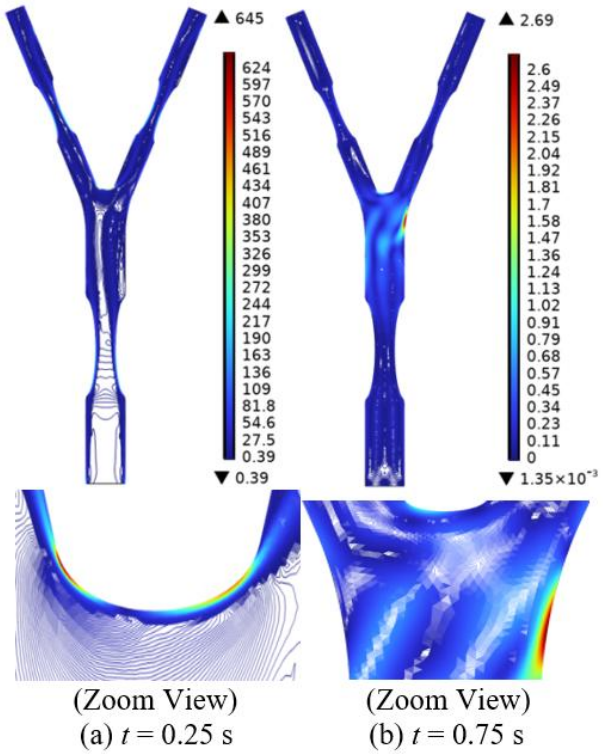

Figure 12. Wall shear stress (WSS) distributions at peak systole (t = 0.25 s) and end diastole (t = 0.75 s) (non-Newtonian)

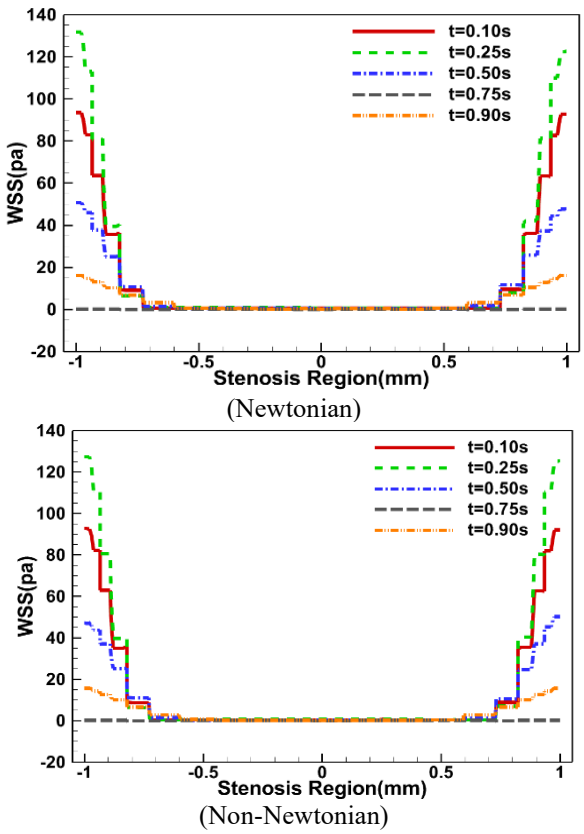

Figure 13. Wall shear stress (WSS) distributions at stenosis throat of parent artery for fluid rheology models at five pulsatile times

Figure 13 shows that the WSS in the central lumen remains close to zero for both the Newtonian and non-Newtonian models across all five evaluated time points. This indicates that shear effects are relatively weak in the central region of the artery, whereas stronger shear stresses are expected near the arterial walls. Among the time points, WSS reaches its maximum magnitude at t = 0.25 s, corresponding to the peak systolic phase, whereas at t = 0.75 s the WSS becomes almost negligible, reflecting the reduced flow acceleration during the later part of the cardiac cycle. The near-zero WSS at t = 0.75 s promotes prolonged particle residence, increasing thrombus risk, while the peak WSS at t = 0.25 s may induce sharp shear gradients, contributing to plaque instability and localized vascular remodeling. Overall, these WSS patterns create a flow environment susceptible to atherosclerosis, thrombosis, and arterial wall weakening [20].

3.4 Oscillatory Shear Index distributions

Figure 14 illustrates the axial variation of the OSI at the stenosis throats of the right and left daughter arteries, comparing Newtonian and non-Newtonian fluid models. OSI exhibits a characteristic dip near the central stenotic region, indicating a predominance of unidirectional flow at the stenosis throat. It then gradually increases along the post-stenotic segments, reflecting the presence of disturbed and oscillatory flow in these regions. Notably, the results obtained for the OSI in the Newtonian and non-Newtonian cases exhibit very similar trends. Only small quantitative discrepancies can be seen between these two approaches, which suggests that the non-Newtonian fluid rheology has little influence on the flow dynamics. The distribution of the shear oscillations is controlled predominantly by the geometry of the artery and the nature of the stenosis.

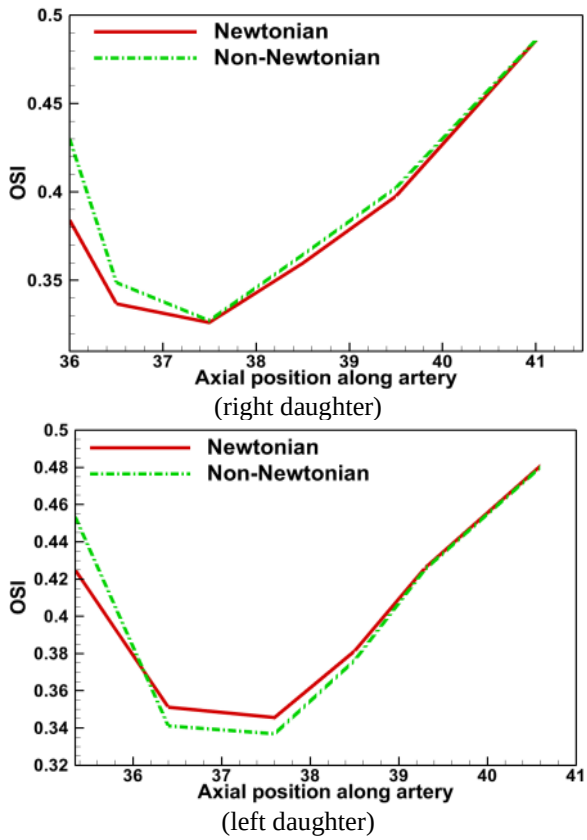

Figure 14. Variation of Oscillatory Shear Index (OSI) at the stenosis throat of right and left daughter arteries for fluid rheology models

Table 3. Quantitative comparison of the key hemodynamic parameters predicted by the Newtonian and non-Newtonian (Carreau) models

Parameter	Newtonian	Non-Newtonian
Peak velocity at (t = 0.25 s)	4.8338 m/s	4.9047 m/s
Peak velocity at (t = 0.75 s)	0.17438 m/s	0.1486 m/s
Pressure drop at (t = 0.25 s)	70 Pa	180 Pa
Pressure drop at (t = 0.75 s)	0.152 Pa	0.273 Pa
Peak wall shear stress (WSS) at (t = 0.25 s)	651 Pa	645 Pa
Peak WSS at (t = 0.75 s)	3.06 Pa	2.69 Pa
Peak Oscillatory Shear Index (OSI) in right daughter artery (0-1 s)	0.4831	0.4817
Peak OSI in left daughter artery (0-1 s)	0.4851	0.4826

Furthermore, elevated OSI downstream of the stenoses, particularly near the bifurcation, indicates regions of highly oscillatory flow. Previous experimental and clinical studies have suggested that such hemodynamic conditions may be associated with endothelial dysfunction and vascular remodeling. These findings provide insight into disturbed hemodynamics associated with cardiovascular disease progression.

Table 3 presents a quantitative comparison of the key hemodynamic parameters obtained from the Newtonian and non-Newtonian (Carreau) models. Both models exhibited similar trends, with only slight differences in velocity, pressure, WSS, and OSI.

4. CONCLUSIONS

The findings show that the occurrence of stenosis in both parent and daughter arteries changes the hemodynamics of the bifurcated artery considerably. The pulsatile nature of the flow, presence of the bifurcating artery, and narrowing of the arteries cause the formation of acceleration of the flow, reduction in pressure, vortex formation, and variation in the WSS. The Newtonian and non-Newtonian models predicted peak systolic velocities of 4.83 m/s and 4.90 m/s, respectively, with corresponding peak pressures of 9.19 kPa and 9.30 kPa. The maximum WSS reached approximately 651 Pa (Newtonian) and 645 Pa (non-Newtonian), while both models predicted similar peak OSI values (≈0.48) in the daughter arteries. A comparative study between the Newtonian and the non-Newtonian models for blood has indicated that the non-Newtonian model gives a smooth distribution of velocities and pressures, lower pressure gradients, and minimal oscillations in the flow. The results indicate that taking into account the shear-thinning nature of blood makes the blood model physiologically realistic.

However, the present study considers a simplified model of coronary artery anatomy, which might not completely represent the individual's specific anatomy and flow dynamics. Future studies will incorporate patient specific geometries and fluid structure interaction (FSI) analysis to improve the physiological relevance and clinical applicability of the findings.

ACKNOWLEDGMENT

The authors gratefully acknowledge the financial support provided by the National Science and Technology (NST) Fellowship, Ministry of Science and Technology, Government of Bangladesh, for conducting this research.

REFERENCES

[1] Nandakumar, N., Sahu, K.C., Anand, M. (2015). Pulsatile flow of a shear-thinning model for blood through a two-dimensional stenosed channel. European Journal of Mechanics - B/Fluids, 49: 29-35. https://doi.org/10.1016/j.euromechflu.2014.07.005

[2] Carvalho, V., Pinho, D., Lima, R.A., Teixeira, J.C., Teixeira, S. (2021). Blood flow modeling in coronary arteries: A review. Fluids, 6(2): 53. https://doi.org/10.3390/fluids6020053

[3] Song, J.F., Kouidri, S., Bakir, F. (2021). Numerical study on flow topology and hemodynamics in tortuous coronary artery with symmetrical and asymmetrical stenosis. Biocybernetics and Biomedical Engineering, 41(1): 142-155. https://doi.org/10.1016/j.bbe.2020.12.006

[4] Jamali, M.S.A., Ismail, Z., Amin, N.S. (2021). Effect of different types of stenosis on generalized power law model of blood flow in a bifurcated artery. Journal of Advanced Research in Fluid Mechanics and Thermal Sciences, 87(3): 172-183. https://doi.org/10.37934/arfmts.87.3.172183

[5] Zhou, Y., Lee, C., Wang, J.Y. (2018). The computational fluid dynamics analyses on hemodynamic characteristics in stenosed arterial models. Journal of Healthcare Engineering, 2018(1): 4312415. https://doi.org/10.1155/2018/4312415

[6] Al-Assi, G., Kadhim Abosaoda, M., Mohaisen Mousa, H., et al. (2026). Impact of non-Newtonian blood rheology on hemodynamics in a realistic coronary artery: A computational fluid dynamics study. Results in Engineering, 30: 111186. https://doi.org/10.1016/j.rineng.2026.111186

[7] Achab, L., Mahfoud, M., Benhadid, S. (2016). Numerical study of the non-Newtonian blood flow in a stenosed artery using two rheological models. Thermal Science, 20(2): 449-460. https://doi.org/10.2298/TSCI130227161A

[8] Athani, A., Ghazali, N.N.N., Badruddin, I.A., et al. (2021). Two-phase non-Newtonian pulsatile blood flow simulations in a rigid and flexible patient-specific left coronary artery (LCA) exhibiting multi-stenosis. Applied Sciences, 11(23): 11361. https://doi.org/10.3390/app112311361

[9] Genuardi, L., Chatzizisis, Y.S., Chiastra, C., et al. (2021). Local fluid dynamics in patients with bifurcated coronary lesions undergoing percutaneous coronary interventions. Cardiology Journal, 28(2): 321-329. https://doi.org/10.5603/CJ.a2020.0024

[10] Colombo, A., Chiastra, C., Gallo, D., et al. (2025). Advancements in coronary bifurcation stenting techniques: Insights from computational and bench testing studies. International Journal for Numerical Methods in Biomedical Engineering, 41(3): e70000. https://doi.org/10.1002/cnm.70000

[11] Ekmejian, A.A., Carpenter, H.J., Ciofani, J.L., et al. (2024). Advances in the computational assessment of disturbed coronary flow and wall shear stress: A contemporary review. Journal of the American Heart Association, 13(19): e037129. https://doi.org/10.1161/JAHA.124.037129
[12] Fernandes, M., Sousa, L.C., António, C.C., Silva, S., Pinto, S.I.S. (2025). A review of computational methodologies to predict the fractional flow reserve in coronary arteries with stenosis. Journal of Biomechanics, 178: 112299. https://doi.org/10.1016/j.jbiomech.2024.112299
[13] Ajayi, N.O., Lazarus, L., Vanker, E.A., Satyapal, K.S. (2013). Anatomic parameters of the left coronary artery: An angiographic study in a South African population. International Journal of Morphology, 31(4): 1393-1398. https://doi.org/10.4067/s0717-95022013000400039
[14] Tzirakis, K., Kamarianakis, Y., Kontopodis, N., Ioannou, C.V. (2023). Classification of blood rheological models through an idealized symmetrical bifurcation. Symmetry, 15(3): 630. https://doi.org/10.3390/sym15030630
[15] Liu, H.P., Lan, L.F., Abrigo, J., et al. (2021). Comparison of Newtonian and non-Newtonian fluid models in blood flow simulation in patients with intracranial arterial stenosis. Frontiers in Physiology, 12: 718540. https://doi.org/10.3389/fphys.2021.718540
[16] Uddin, M.J., Bangalee, M.Z.I., Ferdows, M. (2023). Numerical computation of pulsatile hemodynamics and diagnostic concern of coronary bifurcated artery flow for Newtonian and non-Newtonian fluid. Heliyon, 9(7): e17533. https://doi.org/10.1016/j.heliyon.2023.e17533
[17] Zain, N.M., Ismail, Z. (2017). Modelling of Newtonian blood flow through a bifurcated artery with the presence of an overlapping stenosis. Malaysian Journal of Fundamental and Applied Sciences, 13: 304-309. https://doi.org/10.11113/mjfas.v13n4-1.866
[18] Morel, S., Schilling, S., Diagbouga, M.R., et al. (2021). Effects of low and high aneurysmal wall shear stress on endothelial cell behavior: Differences and similarities. Frontiers in Physiology, 12: 727338. https://doi.org/10.3389/fphys.2021.727338
[19] Kafle, J., Gaire, H.P., Pokhrel, P.R., Kattel, P. (2022). Analysis of blood flow through curved artery with mild stenosis. Mathematical Modeling and Computing, 9(2): 217-225. https://doi.org/10.23939/mmc2022.02.217
[20] Trenti, C., Ziegler, M., Bjarnegård, N., Ebbers, T., Lindenberger, M., Dyverfeldt, P. (2022). Wall shear stress and relative residence time as potential risk factors for abdominal aortic aneurysms in males: A 4D flow cardiovascular magnetic resonance case–control study. Journal of Cardiovascular Magnetic Resonance, 24(1): 18. https://doi.org/10.1186/s12968-022-00848-2

NOMENCLATURE

ρ	density of blood, $\mathrm{kg/m^3}$
τ	viscous stress tensor, Pa
μ	dynamic viscosity, Pa s
$\dot{\gamma}$	shear rate, $\mathrm{s^{-1}}$
L	artery length, mm
WSS	wall shear stress, Pa
LCA	left coronary artery, mm
OSI	oscillatory shear index
FEM	finite element method